DTU Library

Discovery of the Nearly Zero Flux between Two Parallel Conductors in Planar Transformers

Li, Mingxiao; Ouyang, Ziwei; Andersen, Michael A.E.

Published in:
IEEE Transactions on Power Electronics

Link to article, DOI:
10.1109/TPEL.2021.3093171

Publication date:
2022

Document Version
Peer reviewed version

Citation (APA):
Li, M., Ouyang, Z., & Andersen, M. A. E. (2022). Discovery of the Nearly Zero Flux between Two Parallel Conductors in Planar Transformers. *IEEE Transactions on Power Electronics*, *37*(1), 714-723. https://doi.org/10.1109/TPEL.2021.3093171

Discovery of the Nearly Zero Flux between Two Parallel Conductors in Planar Transformers

Mingxiao Li *Student Member, IEEE, Ziwei Ouyang, Senior Member, IEEE and Michael A.E. Andersen, Member IEEE*

***Abstract*-The momentum to achieve high efficiency, high frequency, and high power density in power supplies limits the use of conventional wire-wound transformers, but widely employs planar transformers. Planar transformers intrinsically benefit from low profile, predictable parasitic components, ease of manufacture and excellent repeatability of construction, which are generally applied to high frequency and high current applications, such as data centers and telecoms. Reducing the current density through parallel connections is becoming common practice in planar transformers. However, the current on every parallel conductor is usually unbalanced and hard to be predicted. Start from the motivation to predict parallel current distribution, a phenomenon is discovered in this paper that the parallel current distribution is constant from medium frequency and follows the same pattern in higher frequency range. Besides, this paper points out that the insulation thickness also affects the current distribution. Furthermore, the phenomenon that the magnetic flux in the space between two parallel conductors approaches zero when parallel currents are frequency independent is proved theoretically and demonstrated experimentally. Together with Ampere's circuital law which links the current to the magnetic field, the current distribution can be derived. No complex mathematical calculation or simulation tool is required. Any applications using planar transformers with parallel conductors at medium frequency or higher frequency can adopt this method to predict the parallel current distribution for design optimization.**

I. Introduction

Achieving high efficiency and high power density has become a general requirement for power electronic designs. Among many components in a power supply, the transformer usually takes 30%-50% of the total system volume and creates nearly half of the power loss. Thereby, the transformer design plays a key role in the power supply to satisfy the size and efficiency requirements.

High frequency operation offers a way to shrink the system volume by reducing the size of the passive components. Planar transformers are proved to have excellent performance at high frequency operation [1]-[6]. They are recognized by low profile, predictable parasitic components, ease of manufacture and excellent repeatability of construction. As opposed to conventional wire-wound transformers, planar transformers usually contain windings made of copper sheets etched on a printed circuit board (PCB) in a spiral form, as shown in Fig.1. Primary and secondary windings can with relative ease be heavily interleaved in a manufacturing or automation environment.

In high current and high frequency (up to MHz) applications, there is a tendency that lower output voltage is required for many DC/DC power conversions, like data centers and telecoms [7]-[13]. Connecting several conductors in parallel to reduce the large DC current density is commonly used in planar transformers. Furthermore, planar transformers allow the easy implementation of interleaving winding layouts to balance the current distribution on each parallel conductor at high frequency.

However, the current on each parallel conductor is usually unbalanced, as discussed in [14]. Previous research has been carried out to estimate the planar transformer AC resistance [15]-[19] and core losses [20]-[29]. Studies [24]-[26] utilize finite element analysis (FEA) to investigate several parallel winding layouts. However, this approach is time-consuming and not analytical for optimal design. A lumped circuit model is proposed in paper [27] to predict the AC resistance and leakage inductance. Literature [29] presents a method to derive the currents on parallel conductors. Nevertheless, solutions are hard to be derived for a planar transformer with complex structures and multiple turns in parallel. The investigation over the current distribution at high frequency is not discussed.

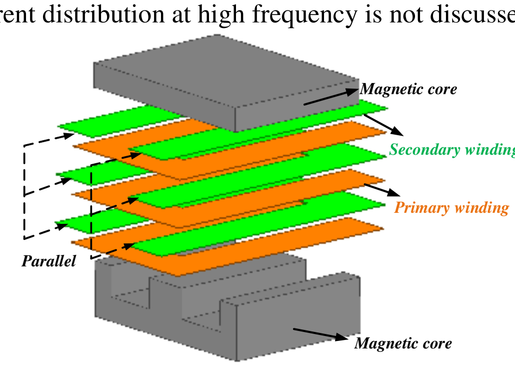

Fig.1 3D view of the planar transformer

In this paper, a phenomenon is discovered that the currents on parallel conductors do not change with frequency from medium frequency and keeps constant at higher frequency. Additionally, previous research usually assumes the identical insulation thickness to analyze planar transformers. However, the insulation thickness usually varies from layer to layer in a practical PCB fabrication. This paper points out that the insulation thickness also affect the parallel current distribution through the comparison between Case I and Case II, as shown in Fig.3. In the worst scenario, the interleaving winding layout has lost its benefit of better current sharing.

The phenomenon that the magnetic flux between two parallel conductors approaches zero when parallel currents are frequency independent are proved theoretically and demonstrated experimentally. Together with Ampere's circuital law, the current distribution can be derived. No complex mathematical calculation or simulation tool is required. Dowell equations can be used to calculate the AC resistance afterward.

Any applications using planar transformers with parallel conductors operating at medium frequency or higher frequency can adopt this method to predict the parallel current distribution for design optimization.

II. Parallel Current Distribution Principle

The analyses given in section follows the "1-D" assumption: the electromagnetic field and current distribution within and around the conductor only vary along the thickness of the conductor (or insulation layer) [15][27]-[29]. The target winding layouts only have one conductor on each layer, and extremely small conductor-to-core clearances compared to the winding width. Besides, the 10% PCB manufacture tolerance, terminations using to measure parallel currents, and the accuracy of the measurement apparatus are not considered. The subsection A presents the theoretical support for the constant parallel current distribution and the cancelled flux at high frequency. The subsection B use simulations and the proposed method to predict parallel current distributions.

A. Theoretical support for the cancelled flux between two parallel conductors

At high frequency operation, eddy current results in large power loss in winding conductors. It can be characterized by skin effect and proximity effect. The proximity effect in parallel conductors is introduced here. Fig.2 illustrates cross-section views of two planar windings. One primary conductor (P) carries high frequency sinusoidal current $i_p(t)$. Two secondary conductors (S_1 and S_2) are short circuited and connected in parallel. These conductors are closely spaced and the spacing between every conductor is identical for each layer. The transformer works in medium frequency or higher frequency. The skin depth is given by

$$\delta=\sqrt{\frac{\rho}{\pi\mu f}} \tag{1}$$

where f is the frequency; μ and ρ are the permeability and the resistivity of the conductor, respectively. For a copper conductor, μ is the same with the air permeability μ_o.

In Fig.2 (a), a high frequency current $i_p(t)$ in conductor P tends to the surface adjacent to conductor S_1 due to the skin effect. A flux $\Phi_1(t)$ is induced in the region between conductors P and S_1. This flux tends to penetrate conductor S_1. Based on Lenz's law, there is a current induced on the upper part of conductor S_1. It attempts to cancel the flux $\Phi_1(t)$. As these conductors are closely spaced, the induced current in conductor S_1 is identical with $i_p(t)$ but in an opposite direction. Furthermore, the total current in secondary conductors is no larger than the primary current using Faraday's law. Thus, no current runs through conductor S_2. Following Ampere's circuital law which links the current to the magnetic field, the magnetic field H is plotted in Fig.2 (a). b is the window width of the magnetic core. It can be observed that there is no magnetic field H in the space between conductors S_1 and S_2. This means magnetic flux $\Phi_2(t)$ between two parallel conductors is zero. The phenomenon is also applied when the primary conductor P is sandwiched between two secondary conductors S_1 and S_2, as shown in Fig.2 (b). The magnetic fluxes induced by the conductor P, $\Phi_1(t)$ and $\Phi_2(t)$, tend to penetrate conductors S_1 and S_2, respectively. $\Phi_1(t)$ and $\Phi_2(t)$ are identical and opposite to each other. Thus, the current induced on the lower part of the conductor S_1 is identical with the current induced on the upper part of the conductor S_2, which is half of the $i_p(t)$.

It can also be concluded that parallel currents are frequency-independent at high frequency from the above-mentioned analysis. For the winding layout shown in Fig.2 (a), the current flowing through conductor S_1 is identical with $i_p(t)$ but in an opposite direction. For the other winding layout shown in Fig.2 (b), each secondary conductor has $i_p(t)/2$.

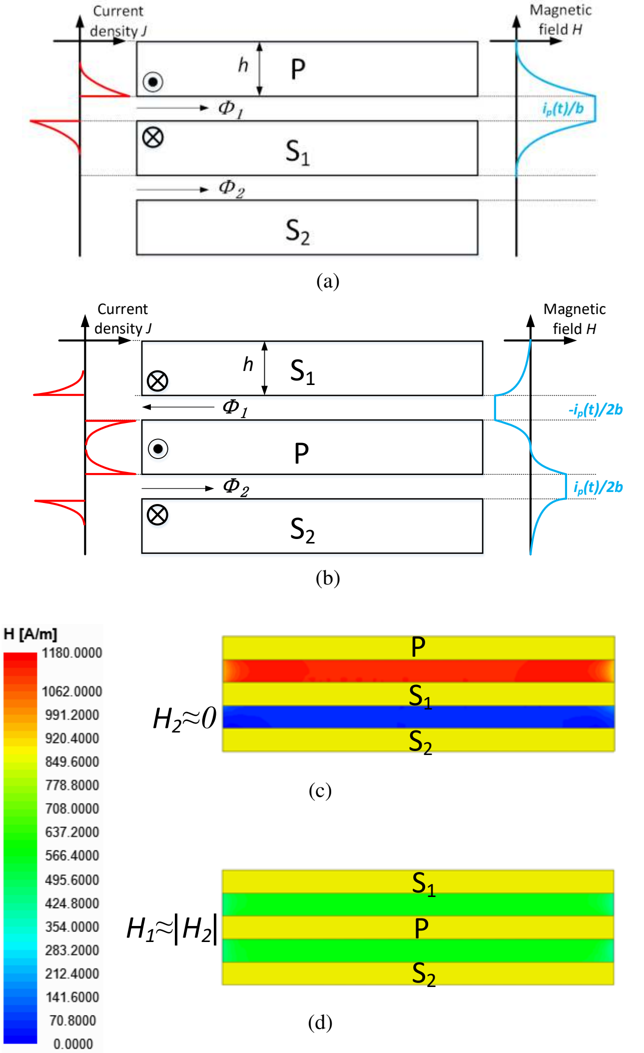

Fig.2 Two transformers (a) non-interleaved and (b) interleaved examples illustrating the proximity effect in parallel conductors. Conductor P carries $i_p(t)$. Conductors S_1 and S_2 are connected in parallel. Simulated H filed at 5MHz in insulation layers for (c) non-interleaved and (d) interleaved windings. The copper thickness is 105μm and the spacing is 100μm for each layer

These two windings, non-interleaved and interleaved winding layouts, are simulated in Ansys Maxwell 2D (finite element analysis) and the corresponding absolute H fields with the same color scale in insulation layers are plotted, as shown in Fig.2 (c) and (d). In Fig.2 (c), the magnetic field H_2

approaches zero and thereby the magnetic flux Φ_2 approximates zero, as the magnetic flux is expressed by

$$\Phi = B \cdot S = \mu_0 H \cdot S \tag{2}$$

where B is flux density; S is the cross-section. In Fig.2 (d), the H_1 and H_2 are identical and opposite to each other, such that the magnetic flux between two parallel conductors $\Phi_1+\Phi_2\approx 0$. Hence, the simulation implies the effectiveness of the theoretical analysis.

From the above-mentioned analysis, it can be conclude that the magnetic flux in the space between two parallel conductors approaches zero at high frequency where eddy current effects dominate. Actually, the magnetic flux is also closing to zero in medium frequency range. The method proposed in the next part to predict the parallel current distribution can be applied to medium frequency. Despite the larger mismatch, it is still acceptable,

B. Proposed approach to predict parallel current distributions

TABLE I
WINDING DETAILS

Parameters	Values
Copper thickness (h)	70µm
Turn ratio (n:1)	2:1
Insulation thickness (t)	0.3mm
Window width (b)	9.275mm
Copper width (b_w)	8.5mm
Resistivity (ρ)	1.71×10^{-8} Ω/m
Air permeability(μ_o)	$4\pi \times 10^{-7}$ H/m
Magnetic core	E32/6/20
Mean turn length (MTL)	20.32mm

This paper also discovers insulation thickness affects the current distribution. Ansys 2D Maxwell is used to simulate the parallel currents for two identical PCB winding layouts $P_1S_2P_2S_1$ shown in Fig.3 (a) and (b). TABLE I illustrates details about the winding arrangement. Secondary conductors S_1 and S_2 are connected in parallel. Primary conductors P_1 and P_2 are in series. A sinusoidal current with the peak value I_p=1A is injected into each primary conductor. The boundary conditions are selected to be balloon. The mesh is also assigned before the simulation starts. The maximum element length is less than the skin depth. The current density is measured at 1 MHz with the same scale. Fig.3 (a) shows Case I with identical insulation thickness t_h=0.3mm for each layer, while Fig.3 (b) shows Case II with different insulation thicknesses. Since Case I and Case II have the same winding layout, the magnetic field H in every insulation layer in Case I is identical with that in Case II.

The currents distributed on S_2 and S_1 as a function of the frequency sweeping from 10kHz to 1GHz are shown in Fig.3 (c) and (d). I_{S1} and I_{S2} are peak currents (at $wt=\pi/2$) on conductors S_1 and S_2, respectively. It can be observed that the same winding layout yields different current distributions due to the different insulation thicknesses. In low frequency (LF) range (30 to 300kHz), the parallel currents are changing with frequency for Case I and Case II. They are becoming gradually stable in medium frequency (MF) range (0.3 to 3MHz), where two parallel conductors always carry the constant current no matter how the frequency changes in each case. In Case I, S_1 and S_2 carry about 1.5A and 0.5A, respectively. In Case II, S_2

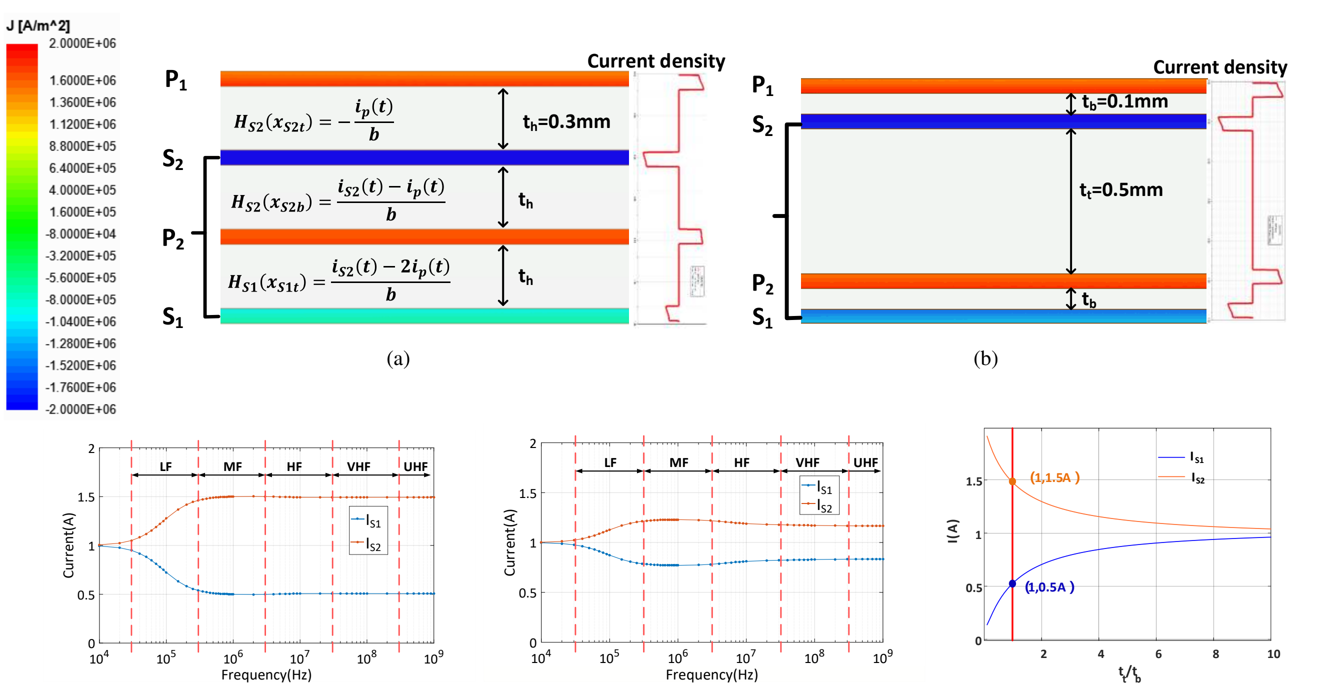

Fig.3 Investigation over the effect of the insulation thickness on parallel current distribution. (a) Case I has identical insulation thickness t_h for each layer. (b) Case II has different insulation thicknesses. Current distributions as a function of frequency from 10kHz to 1GHz are measured for (c) Case I and (d) Case II. From 10kHz to 100kHz, parallel currents I_1 and I_2 are measured every 10kHz. From 100kHz to 1MHz, they are measured every 50kHz. From 1MHz to 10MHz, the scale is 1MHz. From 10 MHz to 100MHz, the scale changes to 10MHz. From 100MHz to 1GHz, the sample scale is 100MHz. (e) I_1 and I_2 versus insulation ratio t_t/t_b with t_t+t_b=0.6mm at 1 MHz

conducts around 1.23A, while S_1 carries 0.77A. In higher frequency ranges, S_1 and S_2 in Case I still keeps constant. Case II shows a small change, but almost follow the same pattern illustrated in medium frequency. S_2 conducts 1.18A and S_1 has 0.82 A.

To further analyze the insulation impact on parallel current distribution at high frequency, I_{S1} and I_{S2} as a function of the insulation ratio t_t/t_b with the constant t_t+t_b=0.6mm are plotted in Fig.3 (e). The frequency is set at 1MHz where the current distribution is obviously constant. It can be observed that the smaller insulation ratio t_t/t_b yields a much higher current on I_2 but lower current on I_{S1}. By contrast, the parallel winding tends to have more uniformly distributed currents with larger insulation ratio t_t/t_b.

From the above analyses, it can be concluded: 1) the parallel current distribution is gradually becoming frequency independent in medium frequency range and still following almost the same pattern in higher frequency ranges; 2) the insulation thickness affects the current distribution.

In order to predict the current distribution with the consideration of the insulation thickness, the discovered phenomena in parallel conductors is used here. No simulation tool or complex calculation is required. For Case I, the magnetic flux in the space between conductors S_1 and S_2 is expressed by

$$\begin{aligned}\Phi_{12} &= \mu_o l t_h\left(H_{S2}\left(x_{S2b}\right)+H_{S1}\left(x_{S1t}\right)\right)\\ &= \frac{\mu_o l t_h}{b}\left(2i_{S2}\left(t\right)-3i_p\left(t\right)\right)\end{aligned} \tag{3}$$

$$H_{S2}\left(x_{S2b}\right)=\frac{i_{S2}\left(t\right)-i_p\left(t\right)}{b} \tag{4}$$

$$H_{S1}\left(x_{S1t}\right)=\frac{i_{S2}\left(t\right)-2i_p\left(t\right)}{b} \tag{5}$$

where μ_o is the air permeability; l is the mean turn length (MTL); b is the window width; $H_{S2}(x_{S2b})$ and $H_{S1}(x_{S1t})$ are magnetic fields in the insulation layer, as shown in Fig.3 (a). $H_{S2}(x_{S2b})$ is the magnetic field along the bottom surface of the conductor S_2; $H_{S1}(x_{S1t})$ is the magnetic field along the top surface of the conductor S_1. Assume the secondary winding perfectly couples with the primary winding. The total secondary current is thus given by

$$i_{S1}\left(t\right)+i_{S2}\left(t\right)=2i_p\left(t\right) \tag{6}$$

where i_{S1}(t) and i_{S2}(t) are the currents on conductors S_1 and S_2 respectively. Using the discovered phenomenon that the magnetic flux in the space between two parallel conductors approaches zero at high frequency, (3) is assigned to be zero. Combining (3) and (6), the parallel currents for Case I are solved by

$$\begin{cases} i_{S_1}\left(t\right)=i_p\left(t\right)/2\\ i_{S_2}\left(t\right)=3i_p\left(t\right)/2\end{cases} \tag{7}$$

Likewise, for Case II, the magnetic flux in the space between conductors S_1 and S_2 is expressed by

$$\begin{aligned}\Phi_{12} &= \mu_o l\left(H_{S2}\left(x_{S2b}\right)t_t+H_{S1}\left(x_{S1t}\right)t_b\right)\\ &= \frac{\mu_o l}{b}\left[i_{S2}\left(t\right)\left(t_t+t_b\right)-i_p\left(t\right)\left(t_t+2t_b\right)\right]\end{aligned} \tag{8}$$

Assign (8) to be zero, and combine (6) and (8). The parallel currents for Case II are solved by

$$\begin{cases} i_{S_1}\left(t\right)=i_p\left(t\right)t_t/\left(t_t+t_b\right)=0.833i_p\left(t\right)\\ i_{S_2}\left(t\right)=i_p\left(t\right)\left(t_t+2t_b\right)/\left(t_t+t_b\right)=1.167i_p\left(t\right)\end{cases} \tag{9}$$

Assume the primary peak current I_p=1A. Recall the simulated current distribution on each parallel conductor at high frequency. The calculation shows excellent agreement with the simulation. Hence, the simulation suggests our finding that the magnetic flux in the space between two parallel conductors approaches zero at high frequency.

The proposed method and discovered phenomena can be applied to any parallel connections and winding layouts. The following part theoretically and mathematically proves our findings.

III. Theoretical and Mathematical Proof for Findings

The current distribution is analyzed in this part based on the same assumptions given initially in Section II.

The current distribution in parallel conductors can be derived by Faraday's law and Kirchhoff's law. The model is illustrated in Fig.4 (a). The magnetic flux Φ_{12} flowing through the space between conductors S_1 and S_2 can be expressed by the current densities (J_1 and J_2) on the surfaces. Additionally, assume the primary windings perfectly couples with secondary windings. The sum of the secondary currents is thus $2i_p(t)$, such that

$$\underbrace{\rho l}_{\Omega\cdot\mathrm{m}^2}\underbrace{\left(J_1-J_2\right)}_{\mathrm{A/m}^2}=\underbrace{jw\Phi_{12}}_{\mathrm{V}} \tag{10}$$

$$i_{S1}\left(t\right)+i_{S2}\left(t\right)=2i_p\left(t\right) \tag{11}$$

where ρ is the conductor resistivity; l is the conductor mean turn length (MTL); J_1 is the current density on the top surface of the conductor S_1; J_2 is the current density on the bottom surface of the conductor S_2; Φ_{12} is the magnetic flux flowing through the loop formed by J_1 and J_2; i_{S1}(t) and i_{S2}(t) are currents on S_2 and S_1, respectively.

The magnetic field inside the conductor is described by the Helmholtz equation.

$$\frac{d^2H_{S2}\left(x\right)}{dx^2}=\gamma^2H_{S2}\left(x\right) \tag{12}$$

where the complex propagation constant γ is

$$\gamma=\frac{1+j}{\delta} \tag{13}$$

A general solution of the Helmholtz equation is

$$H_i\left(x\right)=H_1e^{\gamma x}+H_2e^{-\gamma x} \tag{14}$$

Fig.4 (b) shows an i^{th} conductor in a planar transformer. The center of the coordinate system is located in the center of the magnetic core. x_{it} and x_{ib} are the distances from y-axis to the top and bottom surfaces of the i^{th} conductor, respectively. From the boundary conditions, H_{ib} and H_{it}, the magnetic field in the i^{th} conductor H_i is expressed by

$$\begin{cases} H_i\left(x_{it}\right) = H_1 e^{\gamma x_{it}} + H_2 e^{-\gamma x_{it}} = H_{it} \\ H_i\left(x_{ib}\right) = H_1 e^{\gamma x_{ib}} + H_2 e^{-\gamma x_{ib}} = H_{ib} \end{cases} \tag{15}$$

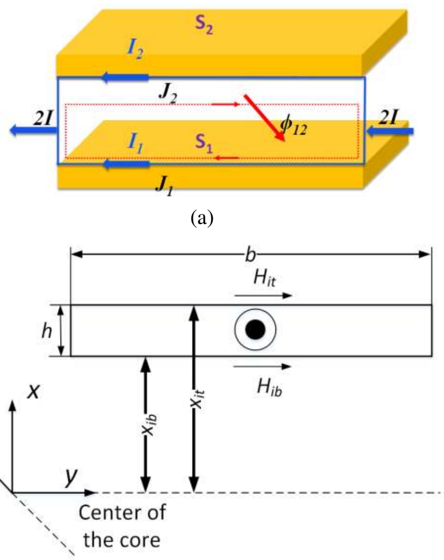

(b)

Fig.4 Theoretical verification of the parallel current distributions. (a) Model of two parallel layers. (b) An i^{th} conductor in a planar transformer.

H_1 and H_2 can be solved by

$$H_1 = H_{it}\frac{\cosh\left(\gamma x_{ib}\right)-\sinh\left(\gamma x_{ib}\right)}{2\sinh\left(\gamma h\right)} + H_{ib}\frac{\sinh\left(\gamma x_{it}\right)-\cosh\left(\gamma x_{it}\right)}{2\sinh\left(\gamma h\right)} \tag{16}$$

$$H_2 = -H_{it}\frac{\sinh\left(\gamma x_{ib}\right)+\cosh\left(\gamma x_{ib}\right)}{2\sinh\left(\gamma h\right)} + H_{ib}\frac{\cosh\left(\gamma x_{it}\right)+\sinh\left(\gamma x_{it}\right)}{2\sinh\left(\gamma h\right)} \tag{17}$$

The magnetic field $H_i(x)$ in the conductor is thus given by

$$H_i\left(x\right) = \frac{H_{it}\sinh\left(\gamma\left(x-x_{ib}\right)\right)-H_{ib}\sinh\left(\gamma\left(x-x_{it}\right)\right)}{\sinh\left(\gamma h\right)} \tag{18}$$

The current density expression for the i^{th} conductor $J_i(x)$ is then derived by

$$J_i\left(x\right) = -\frac{dH_i\left(x\right)}{dx} = \gamma\frac{H_{ib}\cosh\left(\gamma\left(x-x_{it}\right)\right)-H_{it}\cosh\left(\gamma\left(x-x_{ib}\right)\right)}{\sinh\left(\gamma h\right)} \tag{19}$$

In Case I, the magnetic flux Φ_{12} is rewritten here

$$\Phi_{12} = \mu_o l t_h\left(H_{S2}\left(x_{S2b}\right)+H_{S1}\left(x_{S1t}\right)\right) \tag{20}$$

$$H_{S2}\left(x_{S2b}\right) = \frac{i_{S2}\left(t\right)-i_p\left(t\right)}{b} \tag{21}$$

$$H_{S1}\left(x_{S1t}\right) = \frac{i_{S2}\left(t\right)\text{-}2i_p\left(t\right)}{b} = -\frac{i_{S1}\left(t\right)}{b} \tag{22}$$

In Case II, the magnetic flux Φ_{12} is also rewritten here

$$\Phi_{12} = \mu_o l\left(t_t\cdot H_{S2}\left(x_{S2b}\right)+t_b\cdot H_{S1}\left(x_{S1t}\right)\right) \tag{23}$$

Combining (10), (11) and (19) to (23), i_{S1}(t) and i_{S2}(t) for each case can be solved. For Case I, the expressions for i_{S1}(t) and i_{S2}(t)are

$$i_{S1}\left(t\right) = I_p\left(\frac{jw\mu_o t_h\left(\sin\left(wt\right)-\frac{1}{2}\right)\cdot sinh\left(\gamma h\right)}{jwu_o t_h\cdot\sinh\left(\gamma h\right)-\gamma\rho\cdot\cosh\left(\gamma h\right)} - \frac{\gamma\rho\left(\left(\sin\left(wt\right)-\frac{1}{2}\right)\cdot\cosh\left(\gamma h\right)+\frac{1}{2}\right)}{jw\mu_o t_h\cdot\sinh\left(\gamma h\right)-\gamma\rho\cdot\cosh\left(\gamma h\right)}\right) \tag{24}$$

$$i_{S2}\left(t\right) = I_p\left(\frac{\left(\sin\left(wt\right)+\frac{1}{2}\right)\cdot jw\mu_o t_h\cdot sinh\left(\gamma h\right)}{jw\mu_o t_h\cdot\sinh\left(\gamma h\right)-\gamma\rho\cdot\cosh\left(\gamma h\right)} - \frac{\gamma\rho\cdot\left(\left(\sin\left(wt\right)+\frac{1}{2}\right)\cdot\cosh\left(\gamma h\right)-\frac{1}{2}\right)}{jw\mu_o t_h\cdot\sinh\left(\gamma h\right)-\gamma\rho\cdot\cosh\left(\gamma h\right)}\right) \tag{25}$$

For Case II, the expressions for i_{S1}(t) and i_{S2}(t) are

$$i_{S1}\left(t\right) = I_p\left(\frac{jw\mu_o t_t\cdot\left(2\sin\left(wt\right)-1\right)\cdot sinh\left(\gamma h\right)}{jw\mu_o(t_b+t_t)\cdot\sinh\left(\gamma h\right)-2\gamma\rho\cdot\cosh\left(\gamma h\right)} - \frac{\gamma\rho\left(\left(2\sin\left(wt\right)-1\right)\cdot\cosh\left(\gamma h\right)+1\right)}{jw\mu_o(t_b+t_t)\cdot\sinh\left(\gamma h\right)-2\gamma\rho\cdot\cosh\left(\gamma h\right)}\right) \tag{26}$$

$$i_{S2}\left(t\right) = I_p\left(\frac{jw\mu_o\left(2t_b\sin\left(wt\right)+t_t\right)\cdot sinh\left(\gamma h\right)}{jw\mu_o\left(t_b+t_t\right)\cdot\sinh\left(\gamma h\right)-2\cdot\gamma\rho\cdot\cosh\left(\gamma h\right)} - \frac{\gamma\rho(\left(2\sin\left(wt\right)+1\right)\cdot\cosh\left(\gamma h\right)-1)}{jw\mu_o\left(t_b+t_t\right)\cdot\sinh\left(\gamma h\right)-2\cdot\gamma\rho\cdot\cosh\left(\gamma h\right)}\right) \tag{27}$$

Fig.5 (a) and (b) show I_{S1} and I_{S2} as a function of the frequency for Case I and Case II, respectively. The calculated instants I_{S1} and $I_{S2}$are peak currents of (26) and (27), respectively. The theoretical results illustrate excellent agreement with the simulation for Case I. There is a maximum 10% mismatch between the calculation and simulation for Case II, because of the assumption that the primary windings perfectly couples with secondary windings.

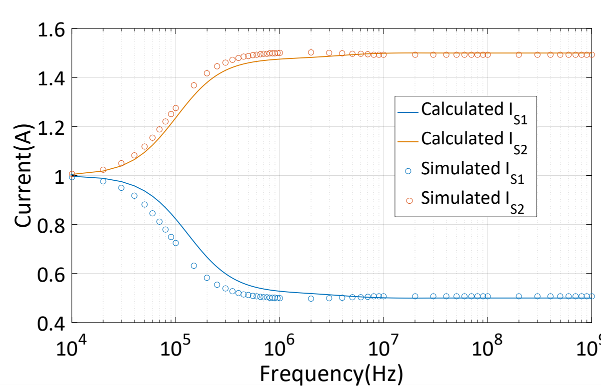

(a)

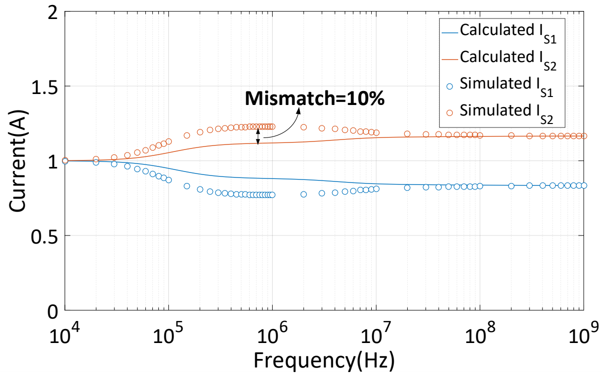

(b)

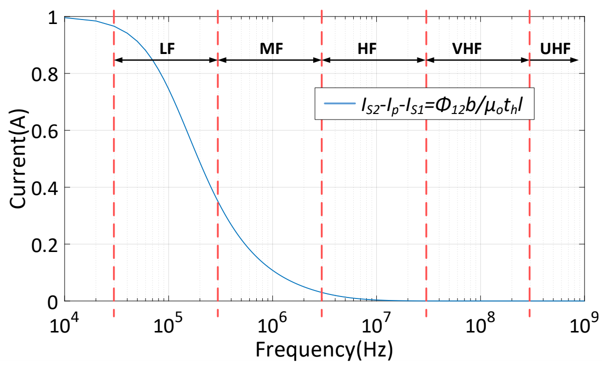

(c)

Fig.5 Comparison between the simulated and calculated current distribution for (a) Case I and (b) Case II. (c)I_{S2}-I_p+I_{S1} versus frequency for Case I

Equations (10) and (11) are not limited to 2 parallel layers, but any parallel connections. However, solving these equations is becoming extremely time-consuming and complex when it comes to multiple turns in parallel and varying insulation thicknesses for each layer. The phenomena and the straightforward method proposed in this paper can be used to predict the parallel current distribution at medium frequency or higher frequency. To suggest our finding, (20), (21) and (22) are rearranged. The new relation among i_{S1}(t), i_{S2}(t), i_p(t) and Φ_{12} can be found, as given in (28).

$$i_{S2}(\mathrm{t}) - i_p(\mathrm{t}) - i_{S1}(\mathrm{t}) = \frac{\Phi_{12} b}{\mu_o t_h l} \tag{28}$$

Equation (28) as a function of the frequency at $wt=\pi/2$ (peak currents) is illustrated in Fig.5 (c). The curve approaches zero as the frequency increases, which implies the effectiveness of our findings.

To further prove our findings can be applied to any parallel connections, two winding layouts are analyzed in the next section.

IV. Demonstrations of the Proposed Theory

The following analyses consider that: 1) the excitation to every primary conductor is a sinusoidal current; 2) the calculated currents are the amplitudes at $wt=\pi/2$; 3) Except for the different insulation thicknesses, other parameters keeps the same with TABLE I. To suggest the effectiveness of our finding, the theory mentioned in Section II is used to predict the current distribution. Two different parallel connections with identical copper thickness h=70μm for each conductor, as shown in Fig.6 (a) and (b), will be discussed in the subsequent part.

For Case III, 4 primary conductors are connected in series, while 4 secondary conductors are in parallel. The currents on primary conductors, namely I_{p1}, I_{p2}, I_{p3}, and I_{p4}, are thus identical. Using the proposed method, as given in (29), the parallel current distribution can be solved.

$$\begin{cases} \Phi_{12} = \mu_o \; l\left(t_{h2} H_{m2} + t_{h3} H_{m3}\right) = 0 \\ \Phi_{23} = \mu_o \; l\left(t_{h4} H_{m4} + t_{h5} H_{m5}\right) = 0 \\ \Phi_{34} = \mu_o \; l\left(t_{h6} H_{m6} + t_{h7} H_{m7}\right) = 0 \\ I_1 + I_2 + I_3 + I_4 = 4 I_p \end{cases} \tag{29}$$

where Φ_{12}, Φ_{23} and Φ_{34} are the magnetic fluxes between conductors S_1 and S_2, S_1 and S_2, and S_3 and S_4, respectively; I_1, I_2, I_3, and I_4 are secondary peak currents on S_1, S_2, S_3, and S_4, separately; I_p is the peak current on each primary conductor. Other quantities can be found in Fig.6 (a) and (b).

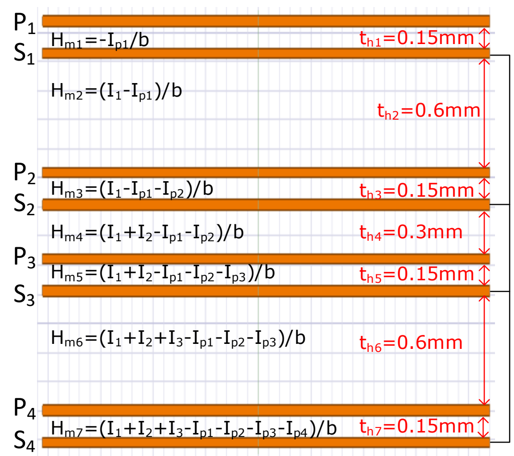

(a)

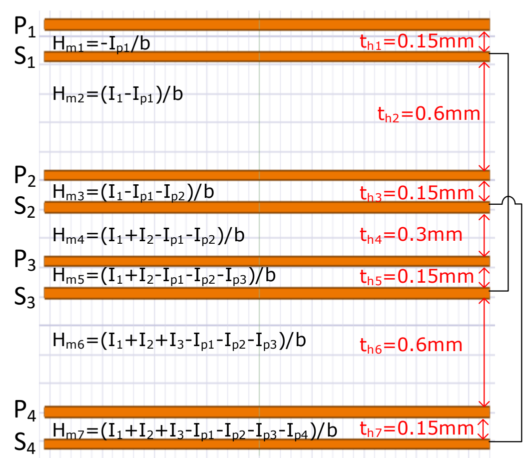

(b)

Fig.6 Two difference winding layouts (a) Case III:a 4:1 winding layout with H field in insulation layer; (b) Case IV: a 4:2 winding layout with H field in insulation layer.

Case IV is a 4:2 winding layout whose primary conductors are in series, and secondary conductors are series-parallel connected. Conductors S_1 and S_3, S_2 and S_4 are in parallel, respectively. 4 parallel currents can be solved from (30) which represents the magnetic fluxes between two parallel conductors and current balances.

$$\begin{cases} \Phi_{13} = \mu_o \ l\left(t_{h2}H_{m2} + t_{h3}H_{m3} + t_{h4}H_{m4} + t_{h5}H_{m5}\right) = 0 \\ \Phi_{24} = \mu_o \ l\left(t_{h4}H_{m4} + t_{h5}H_{m5} + t_{h6}H_{m6} + t_{h7}H_{m7}\right) = 0 \\ I_1 + I_3 = 2I_p \\ I_2 + I_4 = 2I_p \end{cases} \tag{30}$$

To prove the validity of the calculation, TABLE II and TABLE III present the comparisons between the Ansys Maxwell 2D simulation at 1MHz and the calculated results for Case III and Case IV. The total secondary current is less than 4A in simulation as the leakage energy is considered. The proposed method suggests an excellent performance: the calculated parallel current on each conductor illustrates good consistency with the simulation. The maximum mismatch is below 9%, which is primarily due to the assumption that secondary and primary windings are perfectly coupled with each other.

TABLE II
CASE III: COMPARISON BETWEEN SIMULATION AND CALCULATION

Quantities	Simulation (A)	Calculation (A)	Error
I_1	1.229	1.2	2.4%
I_2	1.117	1.133	1.4%
I_3	0.863	0.867	0.5%
I_4	0.74	0.8	8.1%
Total	3.949	4	-

TABLE III
CASE IV: COMPARISON BETWEEN SIMULATION AND CALCULATION

Quantities	Simulation (A)	Calculation (A)	Error
I_1	1.18	1.182	0.17%
I_2	1.2	1.182	1.5%
I_3	0.78	0.818	4.8%
I_4	0.76	0.818	7.6%
Total	3.92	4	-

Acknowledging the current distribution on each conductor, the AC resistance R_{ac} for each case can be determined afterward. The power loss of a conductor is calculated by (31)

$$P = \frac{1}{2}\rho bl\int_{x_m}^{x_n} |J|^2 \, dx \tag{31}$$

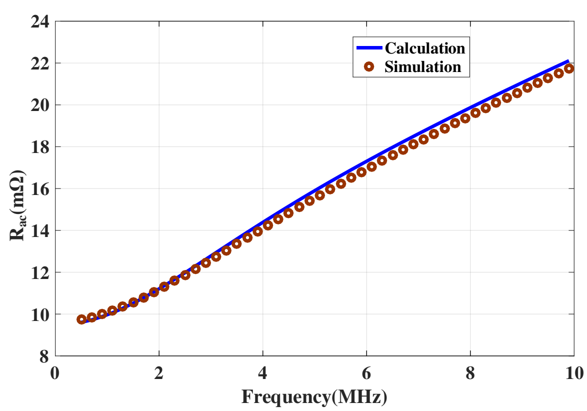

(a)

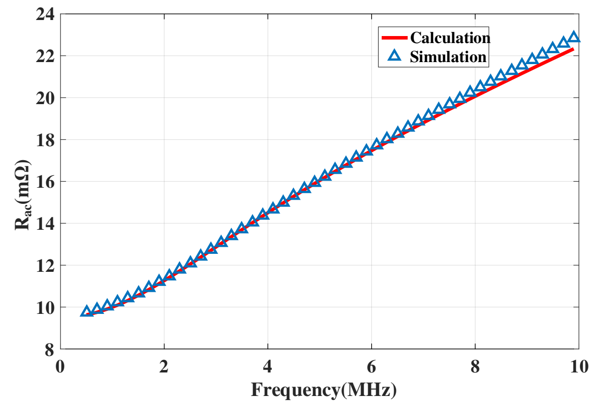

(b)

Fig.7 Comparisons between the calculated AC resistance and simulated AC resistance for (a) Case III and (b) Case IV

Fig.7 shows the calculated AC resistance and simulated AC resistance as a function of frequency for each case. The excellent agreement further proves the effectiveness of the propose method.

TABLE IV
WINDING DETAILS

Parameters	Values
Copper thickness (h)	70µm
Turn ratio (n:1)	2:1
Window width (b)	5.9mm
Winding width (b_w)	4.8mm
Core material	ML91S
Relative permeability of the core(μ_c)	900
Magnetic core	E22/6/16

V. EXPERIMENT

This paper demonstrated the theory presented above in an experiment. The two PCB winding layouts, Case III and Case IV, are fabricated. The magnetic core is E22/6/16. The insulation and copper thickness for each layer keeps almost the same with Fig.6 (a) and (b), respectively, despite the 10% PCB manufacture tolerance. Other details are summarized in TABLE IV. To show the insulation thicknesses satisfy the requirement, the PCB is cut off and the cross-section view captured by the Micromanipulator 2210-LS is presented in Fig.8 (a). The experiment setup is shown in Fig.8 (b) and (c). The bipolar amplifier HSA4101 provides the sinusoidal voltage excitation to the primary winding. Secondary conductors were short circuited. The primary current was measured by the current probe AP015 from Lecory. The bandwidth is up to 50MHz. The current probe CWT 015 Ultramini from PEM was used to measure the secondary current of one conductor. The sensitivity is 200mV/A and the bandwidth ranges from 116Hz to 30MHz.

(a)

(b)

(c)

Fig.8 Details about the (a) experiment setups, (b) the planar transformer with current probes, and (c) PCB cross section view captured by Micromanipulator 2210-LS.

Under the same 4V peak-to-peak sinusoidal voltage excitation, the current waveforms on each secondary conductor at 1MHz for Case III were measured and captured in Fig.9. Currents on conductor S_1 and S_2 shows higher amplitude than currents on conductors S_3 and S_4. The corresponding current amplitudes and the ratios of the peak current on each conductor over the secondary average peak current are documented in TABLE V. Compared with the theoretical calculation, the maximum error is below 7%. Likewise, the same procedure is performed for Case IV. Fig. 10 shows the secondary and primary current waveforms and TABLE VI illustrates the comparison between the experiment and calculation. The maximum mismatch is also below 7%.

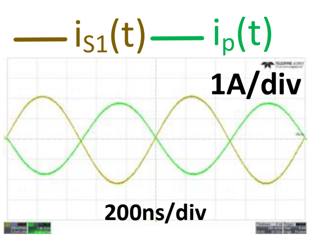

(a)

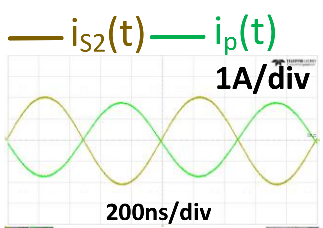

(b)

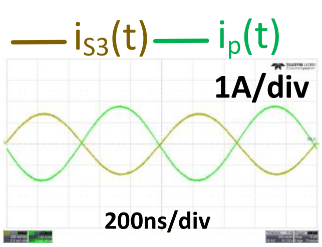

(c)

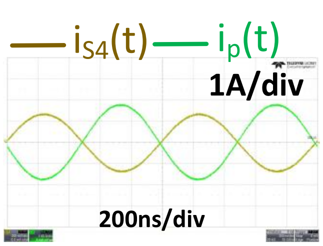

(d)

Fig.9 Current waveforms at 1MHz with 4V voltage excitation for Case III: (a) the current on conductor S_1 and the primary current waveforms. (b)the current on conductor S_2 and the primary current waveforms.(c) the current on conductor S_3 and the primary current waveforms.(d) the current on conductor S_4 and the primary current waveforms

TABLE V
CASE III: COMPARISON BETWEEN EXPERIMENT AND CALCULATION

Peak currents	Experiment (mA)	Experiment ratios ($4I_i/I_{total}$)	Calculation ratios	Error(%)
I_1	2157	1.25	1.2	3.90
I_2	2001	1.15	1.133	2.21
I_3	1407	0.814	0.867	6.41
I_4	1343	0.777	0.8	2.84
Total (I_{total})	6908	-	-	-

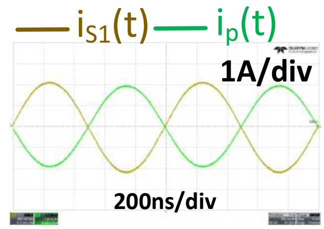

(a)

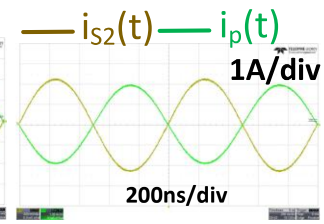

(b)

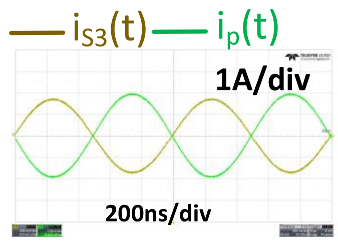

(c)

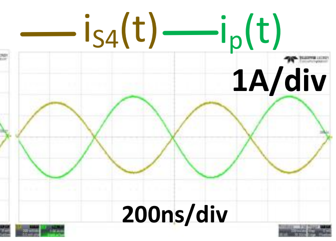

(d)

Fig.10 Current waveforms at 1MHz with 4V voltage excitation for Case IV: (a) the current on conductor S_1 and the primary current waveforms. (b)the current on conductor S_2 and the primary current waveforms.(c) the current on conductor S_3 and the primary current waveforms.(d) the current on conductor S_4 and the primary current waveforms

TABLE VI
CASE IV: COMPARISON BETWEEN EXPERIMENT AND CALCULATION

Peak currents	Experiment (mA)	Experiment ratios ($4I_i/I_{total}$)	Calculation ratios	Error(%)
I_1	2220	1.14	1.2	4.90
I_2	2178	1.12	1.133	1.15
I_3	1711	0.884	0.867	1.65
I_4	1654	0.852	0.8	6.15
Total (I_{total})	7764	-	-	-

To minimize the measurement error, the peak currents are measured at 3 different frequencies, namely 1MHz, 2MHz and 3MHz. The peak parallel currents are measured 4 times with 4 different sinusoidal voltage excitations at every frequency. The average ratios of the peak current on each conductor over the secondary average peak current at every frequency are documented and compared with the calculation, as shown in Fig.11 (a) and (b). The maximum mismatch 8.72% happened to the conductor S_1 at 2MHz for Case III. The comparison for Case IV is represented in Fig.11 (b). The maximum mismatch 8.73% occurs to conductor S_3 at 1MHz. Thus, a mismatch of less than 10% implies that our findings are correct.

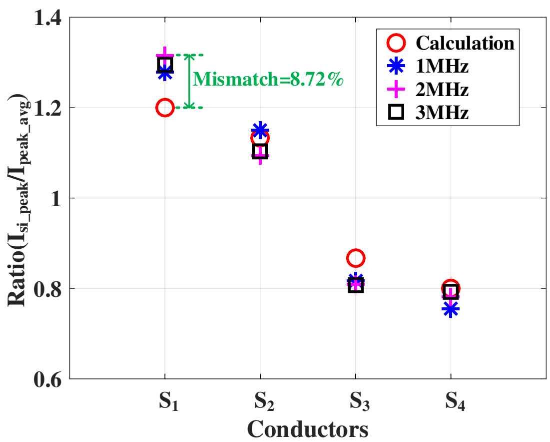

(a)

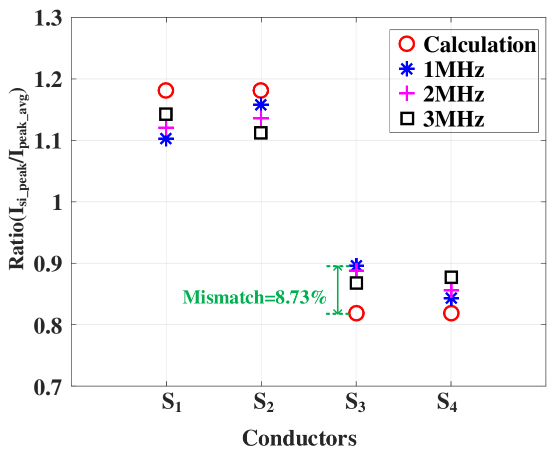

(b)

Fig.11 The comparisons between the calculated current ratios and the measured current ratios at 1MHz, 2MHz and 3MHz are given in (a) Case III and (b) Case IV.

VI. Practical Considerations

A. Copper thickness

The proposed method can be used in a planar transformer with arbitrary insulation thicknesses for each layer. Only one premise is required: the transformer is operating at medium or high frequency where the parallel current becomes independent of frequency. If the copper thickness is much thinner than the skin depth, the parallel currents are varying with frequency. Thereby, the proposed method cannot be applied to predict the parallel current distribution.

B. Conductor-to-core clearances

In practical fabrications of PCBs, clearances have to be inserted between conductors and PCB edges. These clearances influence the dissipated loss and accumulate the reactive energy. Throughout the discussion, this paper focus on winding layouts which have only one conductor on each layer, and extremely small conductor-to-core clearances compared to winding width. Thus, the contribution of edge effects can be neglected[27].

C. Air gaps

Fringing effects induced by air gaps change the current distribution and lead to a mismatch between calculation and experiment. However, fringing effects have negligible influence when conductors are located away from air gaps. In Literature [30], it concludes that air gaps have insignificant influence if the spacing between the gap and the conductor is at least one forth larger than the window width.

D. Measurement

In the theoretical analysis, the PCB manufacture tolerance, terminations using to measure the parallel currents, and the accuracy of the measurement apparatus are not considered. However, these factors may lead to the mismatch in the experiment.

VII. Conclusions

This paper predict the parallel current distribution in planar transformers. This paper present the findings that the parallel current is gradually becoming constant in medium frequency and still following almost the same pattern in higher frequency ranges, and it is also dependent by the insulation thickness. The phenomenon that the magnetic flux between two parallel conductors is close to zero from medium frequency is proposed theoretically and demonstrate experimentally that. Together with Ampere's circuital law, the parallel current distribution for planar transformers at high frequency can be derived. This approach does not require complex mathematical calculation or simulation tools. Any applications using planar transformers with parallel conductors at medium or higher frequency can adopt this method to effectively predict the parallel current distribution for design optimization.

References

[1] M. T. Quirke, J. J. Barrett, and M. Hayes, “Planar magnetic component technology—A review,” *IEEE Trans. Compon. Hybrids, Manuf. Technol.*,vol. 15, no. 5, pp. 884–892, Oct. 1992.

[2] D. J. Perreault, J. Hu, J. M. Rivas, Y. Han, O. Leitermann, R. C. N. PilawaPodgurski, A. Sagneri, and C. R. Sullivan, “Opportunities and challenges in very high frequency power conversion,” in *Proc. IEEE Appl. Power Electron. Conf. Expo.*, Feb. 2009, pp. 1–14.

[3] A. M. Urling, V. A. Niemela, G. R. Skutt, and T. G. Wilson, “Characterizing high-frequency effects in transformer windings—A guide to several significant papers,” in *Proc. IEEE Appl. Power Electron. Conf. Expo.*, Mar. 13–17, 1989, pp. 373–385.

[4] Z. Ouyang, W. G. Hurley, and M. A. Andersen, “Improved Analysis and Modeling of Leakage Inductance for Planar Transformers,” IEEE Journal of Emerging and Selected Topics in Power Electronics, vol. 7, no. 4, pp. 2225–2231, 2019.

[5] Z. Ouyang and M. A. E. Andersen, “Overview of planar magnetic technology—Fundamental properties,” IEEE Trans. Power Electron., vol. 29, no. 9, pp. 4888–4900, Sep. 2014.

[6] W. G. Hurley and M. C. Duffy, “Calculation of self and mutual impedances in planar magnetic structures,” IEEE Trans. Magn., vol. 31, no. 4, pp. 2416–2422, Jul. 1995.

[7] M. Li, Z. Ouyang, and M. A. Andersen, “A Hybrid Multitrack-Sigma Converter with Integrated Transformer for Wide Input Voltage Regulation,” 2020 IEEE Applied Power Electronics Conference and Exposition (APEC), 2020.

[8] C. Fei, M. H. Ahmed, F. C. Lee, Q. Li, "Two-stage 48V-12V/6V1.8V Voltage Regulator Module with Dynamic Bus Voltage Control for Light Load Efficiency Improvement," in IEEE Transactions on Power Electronics , vol.32, no.7, pp.5628-5636

[9] M. Chen, K. K. Afridi, S. Chakraborty and D. J. Perreault, "Multitrack Power Conversion Architecture," IEEE Trans. Power Electron., vol. 32, no. 1, pp. 325-340, Jan. 2017.

[10] X. Wu, H. Shi, “High Efficiency High Density 1 MHz 380–12 V DCX With Low FoM Devices,” IEEE Transactions on Industry Electronics, Volume 67, Issue 2 , Feb 2020.

[11] Y. Ren, M. Xu, K. Yao, and F. Lee, “Two-stage 48 V power pod exploration for 64-bit microprocessor,” *in Proc. IEEE Appl. Power Electron. Conf. and Expo.,* Miami Beach, USA, 9-13 Feb.2003

[12] X. Wu, H. Chen and Z. Qian, "1-MHz LLC Resonant DC Transformer (DCX) With Regulating Capability," IEEE Transactions on Industrial Electronics, vol. 63, pp. 2904-2912, May 2016.

[13] D. Huang, S. Ji, and F. C. Lee, “LLC resonant converter with matrix transformer,” IEEE Trans. Power Electron., vol. 29, no. 8, pp. 4339–4347, Aug. 2014.

[14] X. Margueron, A. Besri, Y. Lembeye, and J.-P. Keradec, “Current sharing between parallel turns of a planar transformer: Prediction and improvement using a circuit simulation software,” IEEE Trans. Ind. Appl., vol. 46, no. 3, pp. 1064–1071, May/Jun. 2010.

[15] P. L. Dowell, “Effects of eddy currents in transformer windings,” Proc. Inst. Electr. Eng., vol. 113, no. 8, pp. 1387–1394, Aug. 1966

[16] J. Hu and C. R. Sullivan, “AC resistance of planar power inductors and the quasidistributed gap technique,” IEEE Trans. Power Electron., vol. 16,no. 4, pp. 558–567, Jul. 2001.

[17] W. G. Hurley, E. Gath, and J. G. Breslin, “Optimizing the AC resistance of multilayer transformer windings with arbitrary current waveforms,” IEEE Trans. Power Electron., vol. 15, no. 2, pp. 369–376, Mar. 2000.

[18] W. G. Hurley and M. C. Duffy, “Calculation of self and mutual impedances in planar magnetic structures,” IEEE Trans. Magn., vol. 31, no. 4, pp. 2416–2422, Jul. 1995.

[19] J. Hu and C. R. Sullivan, “AC resistance of planar power inductors and the quasidistributed gap technique,” IEEE Trans. Power Electron., vol. 16, no. 4, pp. 558–567, Jul. 2001.

[20] (core loss)Y. Han, G. Cheung, A. Li, C. R. Sullivan, and D. J. Perreault, “Evaluation of magnetic materials for very high frequency power applications,” IEEE Trans. Power Electron., vol. 27, no. 1, pp. 425–435, Jan. 2012.

[21] J. Muhlethaler, J. Biela, J. W. Kolar, and A. Ecklebe, “Core losses under the DC bias condition based on Steinmetz parameters,” IEEE Trans. Power Electron., vol. 27, no. 2, pp. 953–963, Feb. 2012.

[22] J. Li, T. Abdallah, and C. R. Sullivan, “Improved calculation of core loss with nonsinusoidal waveforms,” in Proc. IEEE Annu. Meet. Ind. Appl. Soc., Sep. 2001, vol. 4, pp. 2203–2210.

[23] C. P. Steinmetz, “On the law of hysteresis,” Proc. IEEE, vol. 72, no. 2, pp. 197–221, Feb. 1984

[24] A. F. Goldberg, J. G. Kassakian, and M. F. Schlecht, “Finite-element analysis of copper loss in 1–10 MHz transformers,” IEEE Trans. Power Electron., vol. 4, no. 2, pp. 157–167, Apr. 1989.

[25] N. Y. Abed and O. A. Mohammed, “Physics-based high-frequency transformer modeling by finite elements, IEEE Trans. Magn., vol. 46, no. 8, pp. 3249–3252, Aug. 2010.

[26] R. Asensi, R. Prieto, J. A. Cobos, and J. Uceda, “Modeling high frequency multiwinding magnetic components using finite-element analysis,” IEEE Trans. Magn., vol. 43, no. 10, pp. 3840–3850, Oct. 2007.

[27] M. Chen, M. Araghchini, K. K. Afridi, J. H. Lang, C. R. Sullivan and D. J. Perreault, "A Systematic Approach to Modeling Impedances and Current Distribution in Planar Magnetics," in IEEE Transactions on Power Electronics, vol. 31, no. 1, pp. 560-580, Jan. 2016.

[28] R. W. Erickson and D. Maksimovic, “Basic magnetics theory,” in, *Fundamentals of Power Electronics*. Boston, MA, USA: Kluwer,2001.

[29] Wei Chen, Yipeng Yan, Yuequan Hu and Qing Lu, "Model and design of PCB parallel winding for planar transformer," in IEEE Transactions on Magnetics, vol. 39, no. 5, pp. 3202-3204, Sept. 2003.

[30] J. Hu and C. R. Sullivan, “AC resistance of planar power inductors and the quasi-distributed gap technique,” *IEEE Trans. Power Electron.*, vol. 16,no. 4, pp. 558–567, Jul. 2001.